Collisions of droplets on spherical particles

Georgios Charalampous, and Yannis Hardalupas

Citation: Physics of Fluids **29**, 103305 (2017); doi: 10.1063/1.5005124
View online: http://dx.doi.org/10.1063/1.5005124
View Table of Contents: http://aip.scitation.org/toc/phf/29/10
Published by the American Institute of Physics

Articles you may be interested in

Drop impact on spherical soft surfaces
Physics of Fluids **29**, 082106 (2017); 10.1063/1.4996587

Why do we live for much less than 100 years? A fluid mechanics view and approach
Physics of Fluids **29**, 081903 (2017); 10.1063/1.4998717

Droplet impact onto a solid sphere: Effect of wettability and impact velocity
Physics of Fluids **29**, 062111 (2017); 10.1063/1.4990088

Drag reduction using wrinkled surfaces in high Reynolds number laminar boundary layer flows
Physics of Fluids **29**, 093605 (2017); 10.1063/1.4995566

The regime of large bubble entrapment during a single drop impact on a liquid pool
Physics of Fluids **29**, 092101 (2017); 10.1063/1.4992124

High-speed oblique drop impact on thin liquid films
Physics of Fluids **29**, 082108 (2017); 10.1063/1.4996588



Collisions of droplets on spherical particles

Georgios Charalampous and Yannis Hardalupas
Mechanical Engineering Department, Imperial College London, London SW7 2AZ, United Kingdom

(Received 17 May 2017; accepted 15 September 2017; published online 17 October 2017)

Head-on collisions between droplets and spherical particles are examined for water droplets in the diameter range between 170 μm and 280 μm and spherical particles in the diameter range between 500 μm and 2000 μm. The droplet velocities range between 6 m/s and 11 m/s, while the spherical particles are fixed in space. The Weber and Ohnesorge numbers and ratio of droplet to particle diameter were between $92 < We < 1015$, $0.0070 < Oh < 0.0089$, and $0.09 < \Omega < 0.55$, respectively. The droplet-particle collisions are first quantified in terms of the outcome. In addition to the conventional deposition and splashing regimes, a regime is observed in the intermediate region, where the droplet forms a stable crown, which does not breakup but propagates along the particle surface and passes around the particle. This regime is prevalent when the droplets collide on small particles. The characteristics of the collision at the onset of rim instability are also described in terms of the location of the film on the particle surface and the orientation and length of the ejected crown. Proper orthogonal decomposition identified that the first 2 modes are enough to capture the overall morphology of the crown at the splashing threshold. © *2017 Author(s). All article content, except where otherwise noted, is licensed under a Creative Commons Attribution (CC BY) license (http://creativecommons.org/licenses/by/4.0/).* https://doi.org/10.1063/1.5005124

NOMENCLATURE

D	= Droplet diameter
D_0	= Particle diameter
h	= Crown height (base to tip)
Oh	= Ohnesorge number
Re	= Reynolds number, based on D
s	= Arc of film spread on the particle surface
U	= Droplet velocity
We	= Weber number, based on D
Ω	= Droplet to particle diameter ratio
ϕ	= Angle between the vertical direction and the crown base
μ	= Liquid viscosity
θ	= Ejection angle between the crown and the horizontal direction
ρ	= Liquid density
σ	= Surface tension
ζ	= Deflection angle between the crown and the normal direction to the particle surface

I. INTRODUCTION

The spray drying process is widely used to convert liquid slurry to dry particles for the manufacture of a range of products, including foodstuffs, like instant coffee and powdered milk, household detergents, pharmaceuticals, or carbide particles for the manufacture of cutting tools (Masters, 1991). The process is energy intensive. Only in the UK it was estimated that around 1986 about 500 000 ton of coal equivalent were consumed every year for spray drying (Mercer, 1986). It was also estimated that on average around 29% of the energy supplied to spray dryers was wasted (Baker and McKenzie, 2005). Additional reduction in efficiency comes from the production of powder that falls outside the desired size range and needs to be recycled.

During spray drying liquid droplets and dried or semi-dried particles collide with each other. It is also possible that the droplets or particles collide with particles deposited on the wall of the spray dryer. In such cases, there is a possibility of merging, splashing, or ripping of the deposited particle from the wall. Depending on the spray dryer operation, for example, in a swirling flow configuration, the rate of collisions can be significant (Huntington, 2004). This can alter the final powder size and, as a result, the process can become less efficient since the probability of powder particles that fall outside the desired size range increases.

In the case of collisions between droplets, the interface is fluid, curved, and of finite spatial extent. The outcomes of such collisions have been classified by many authors in various categories (Brenn and Frohn, 1989; Orme, 1997; and Qian and Law, 1997). During coalescence, Fig. 1(a), the two droplets merge to form a larger droplet. During bouncing, Fig. 1(b), the two droplets that collide separate without merging and maintain their initial diameters. In reflexive separation, Fig. 1(c), two droplets collide head on or nearly head on. During the collision, they form a disc on the plane of impact. As the disc retracts quickly, it forms an elongating cylinder from which two drops are ejected in the direction of the original droplet directions. Smaller droplets are formed along the length of a filament that disintegrates during separation. In stretching separation, Fig. 1(d), there is an off-axis collision of the two droplets, which initially merge to form an elongated liquid lump. The momentum of the initial droplets is not dissipated during impact and two smaller droplets are released from the

 © Author(s) 2017

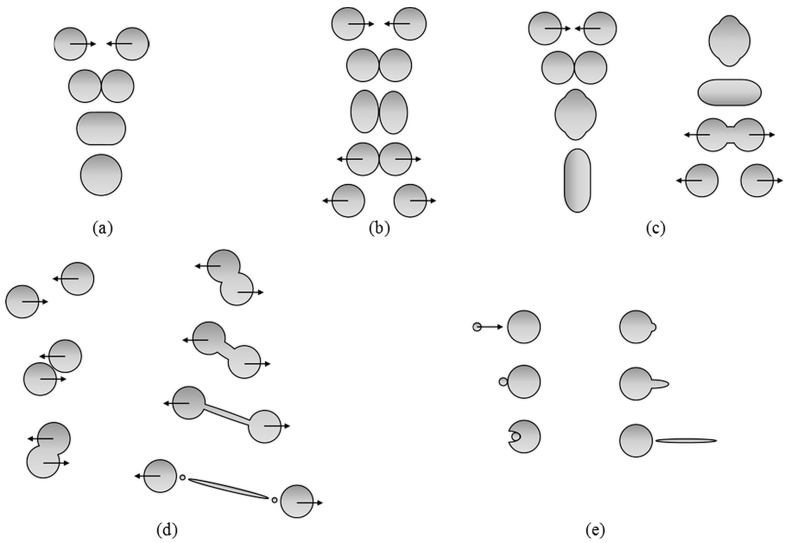


FIG. 1. Regimes of droplet-droplet collision: (a) coalescence, (b) bouncing, (c) reflexive separation, (d) stretching separation, and (e) penetration.

lump in the direction of the initial droplets. A filament that is formed as they separate produces smaller satellite droplets as it breaks up. In cases where the ratio of the droplet diameters is over 4, it is possible that the small droplet penetrates the larger droplet and a jet is formed at the opposite side of the larger droplet (Podvysotsky and Shraiber, 1984).

On the other hand, collisions of droplets with particles are not well understood. Much work has been conducted on collisions with flat surfaces (Chandra and Avedisian, 1991; Mundo *et al.*, 1995; Cossali *et al.*, 1997; Roisman *et al.*, 2006; and Yarin, 2006). In this case, the impact interface is rigid but flat and for all practical purposes can be considered to have infinite extent. The collision outcomes have been systematically classified for both dry and wet surfaces. For dry surfaces (Rioboo *et al.*, 2001; 2002), in prompt splash, Fig. 2(a), the droplet expands radially along the surface in a thin film with the leading edge disintegrating. In crown splash, Fig. 2(b), a crown is formed with a thick rim that breaks up as cusps are formed. If the droplet does not break up as it collides, cohesion forces dominate, which tends to restore the original spherical shape as the deformed liquid retracts. During this phase, receding breakup can occur, Fig. 2(c). If the liquid fully contracts without breaking up, all of the liquid can rebound as a single droplet, Fig. 2(d), or a fraction partially as a smaller droplet with the remaining fraction of the liquid staying attached on the surface, Fig. 2(e). Another possibility is that the droplet will simply deposit on the surface without either breaking or rebounding, Fig. 2(f). If the flat surface is wet, the film presence interferes with the evolution of the phenomenon (Cossali *et al.*, 1997; Wang and Chen, 2000; Rioboo *et al.*, 2003; Yarin, 2006; and Liang and Mudawar, 2016). The impingement outcomes in this case can be rebounding, deposition, prompt splash, and crown splash, which are similar to those described for impact on dry surfaces. However, the details of the development and the mechanisms involved can be significantly different than for impingement on dry surfaces.

When droplets collide with solid particles, the impact surface is rigid, curved, and of finite extent. While this case is

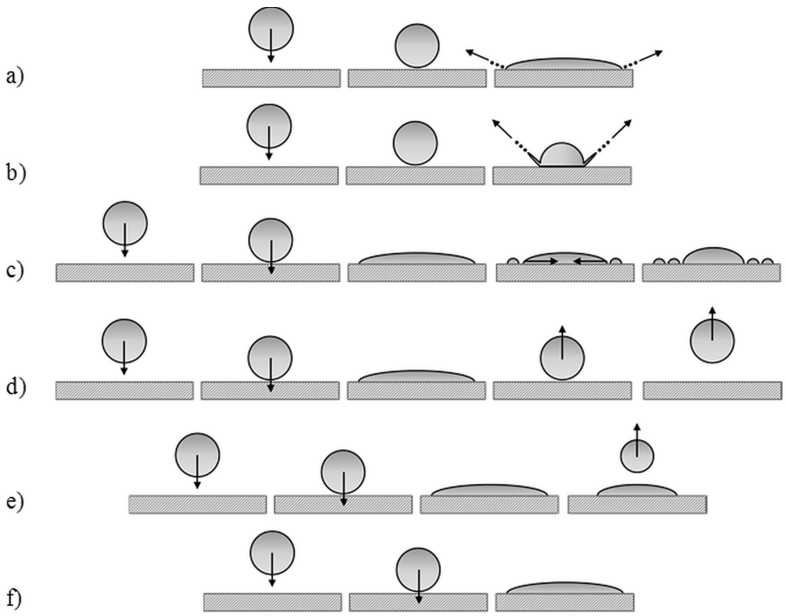


FIG. 2. Regimes of droplet impingement on wall. (a) Prompt splash, (b) crown splash, (c) receding breakup, (d) rebound, (e) partial rebound, and (f) deposition.

somehow between the cases of collisions between droplets and collisions of droplets on flat surfaces, it is not possible to infer the outcomes in this case directly from interpolation. A limited number of investigations exist on this topic.

In the experimental work of Hardalupas *et al.*, 1999 the threshold between splashing and deposition was investigated for droplets in the 160–230 μm diameter range and solid spheres in the 0.8–1.3 mm diameter range. The authors suggest that the splashing threshold is affected by the curvature of the solid particle and proposed a modification of the splashing threshold for collisions of droplets on flat surfaces, which accounts for the curvature of the solid particle.

Bakshi *et al.* (2007) investigated the deposition of a liquid droplet on a particle, for droplets in the 2.4–2.6 mm range and spherical particles between 3.2 mm and 15 mm for 3 different kinds of liquids. The Weber number of their study did not exceed 300. They analysed the temporal and spatial development of the film both experimentally and analytically and classified the development in 3 distinct phases: the initial drop deformation phase, during which the droplet shape remains unaffected by contact with the particle, the inertia dominated phase, for which the viscous forces have little influence, and the viscosity dominated phase, during which the development is governed by the balance of the viscous and gravity forces.

Liang *et al.* (2014) investigated experimentally the impingement of droplets with a diameter of about 1.8 mm on solid spheres with a diameter range of 4 mm–20 mm. They found that the splashing threshold is influenced by the solid sphere-drop diameter ratio. The ratio of the area covered by the liquid film was shown to increase by decreasing the droplet/particle curvature ratio, while the Weber number was found to have only a minor effect.

Pawar *et al.* (2016) considered the collisions of droplets with a diameter of 2.9 mm with particles with diameters of 2.5 mm or 4.0 mm, respectively, in the Weber number range between 0.34 and 52. The collision outcomes were classified as either agglomeration, where the whole particle being engulfed by the droplet, or stretching separation, where only part of the liquid droplet attaches to the particle after the collision. Formation of satellite droplets was also reported. The collision outcomes were mapped in terms of the Weber number and the impact parameter, which is defined at the moment of impact as the ratio of the distance between the centres of the two droplets projected on the normal of the relative velocity vector to the distance between the centres of the droplets. The impact parameter obtains the value of 0 for head-on collisions and 1 for grazing collisions. The transition boundary between agglomeration and stretching separation was found to scale inversely with the Weber number.

The interaction of two simultaneous collisions of a 225 μm diameter monosized droplet streams on a 1.3 mm diameter spherical particle was examined by Barnes *et al.* (1999). A hump of liquid was generated between the two impacting droplets due to the interference of the individual crowns of the two droplets. The droplets generated from the hump breakdown were found to be considerably slower than the droplets produced by the crown breakdown.

Here a new investigation is conducted, which considers collisions of droplets on spherical particles for droplet diameters in the range of 170 μm–280 μm, particle diameters in the range of 0.5–2.0 mm, and collision velocities in the range of 6 m/s–11 m/s. The size and velocity of the droplets are similar to the droplet size produced by atomisers in spray dryers, while the size of the particles is characteristic of detergent particle formulations.

The aim is to extend the limited research, reported in the literature, on droplet-particle collisions, identify the resulting regimes of such collisions, determine their boundaries, and find suitable parameters to describe the outcomes. Additionally, the development of the crown that is produced during the droplet-particle collision is analysed and information related to the initiation of breakup of the crown is obtained, which can be useful for the control of the agglomeration and growth of particles and the development of numerical models and control of coating industrial processes.

This paper is structured in the following order. The experimental arrangement is presented in Sec. II. The results are presented and discussed in Sec. III, which comprises 4 subsections focusing on collision outcomes, the splashing threshold, the characteristics of the crown at the onset of rim instability, and the overall morphology of the crown at the splashing threshold. This paper closes with a summary of the main conclusions.

II. EXPERIMENTAL ARRANGEMENT AND METHODS

Monosized droplets were generated by an in-house built ultrasonic droplet generator. In this approach, a laminar liquid jet is generated by injecting the working liquid through an orifice with an exit diameter of the order of 100 μm at the end of a straight channel. The channel is subject to vibrations from a piezoelectric element attached on the wall along its length; as a consequence, the liquid jet is stimulated by the pulsation frequency and breaks up in a stream of regular size droplets (Schneider and Hendricks, 1964; Schneider *et al.*, 1965; and Brenn *et al.*, 1996). The design used here has been used in a number of previous investigations (Barnes *et al.*, 1999; Hardalupas *et al.*, 1999; and Pergamalis, 2002).

The liquid was supplied to the droplet generator from a pressurized kettle (Alloy Products Corporation). This approach has the advantage that there are no pump-induced vibrations, which interfere with the induced vibrations of the piezoelectric element. The liquid was passed through a 0.5 μm in-line filter to guarantee that the droplets were free from impurities and was delivered to the droplet generator through a stainless steel tube (with the exemption of a small final length which was necessarily a flexible hose) for fast response when adjusting the liquid flowrate. The diameter of the orifice at the exit of the mono-dispersed droplet generator was 100 μm. The resulting diameter of the generated water droplets was between 170 μm and 280 μm, depending of the injection pressure and the oscillation frequency of the piezoelectric element according to

$$D = \left(\frac{6\dot{Q}}{\pi f}\right)^{1/3}, \tag{1}$$

where $\dot{Q}$ is the liquid flowrate and f is the excitation frequency. The droplet generator was operated at 10 000 Hz,

TABLE I. Physical properties of the droplets (20 °C).

ρ (kg/m^3)	998
σ (N/m)	0.073
μ (Pa s)	1.0×10^{-3}

15 000 Hz, and 20 000 Hz to produce the droplets of this investigation. The separation between successive droplets was at minimum 2 droplet diameters and could exceed 5 droplet diameters, depending on the droplet velocity. Therefore, no significant interaction between successive droplets is expected.

The working liquid in this investigation was distilled water. This ensured that its physical properties did not change throughout the duration of the measurement campaign. In addition, the absence of minerals in distilled water was essential in preventing the build-up of deposits on the surface of the spherical particle target. A summary of the physical properties of distilled water is given in Table I.

The spherical particles were made of glass and supported on steel rods. The contact angle between distilled water and glass was measured between 59° and 67°. This is somewhat lower than the 70°–80° range for water on glass contact angle reported by Pawar *et al.* (2016). Three particle diameters, D_0, were considered, namely, 500 μm, 1000 μm, and 2000 μm, making the particle greater than the diameter of the colliding droplet. In this approach, collisions result in droplet spreading on the particle surface. The opposite would result in the particle penetrating the droplet, which is not the case here. The maximum diameter tolerance was better than 3 μm, and the sphericity of the particle target was within 1 μm according to the manufacturer. The surface roughness of the particles was measured by a Wyko Veeco NT9100 optical profiling system with vertical resolution better than 0.1 nm and was found to be about 35 nm. By using smooth particles, the influence of the surface roughness is low, thus reducing the complexity of the interpretation of the measurements. Also, since research of droplet-particle collisions is generally limited to smooth particles, comparison of the results obtained here with the results of previous investigations [for example, Liang *et al.* (2014) considered particles with surface roughness less than 50 nm] is made possible. Finally, even for investigations with ultimate interest in spray drying applications, smooth glass particles have also been used in the past (Pawar *et al.*, 2016).

Imaging was accomplished by a CCD camera (model PCO Sensicam QE). The camera sensor resolution is 1376 × 1040 pixels. The camera was fitted with a long distance microscope (Questar QM-1) to obtain high resolution images

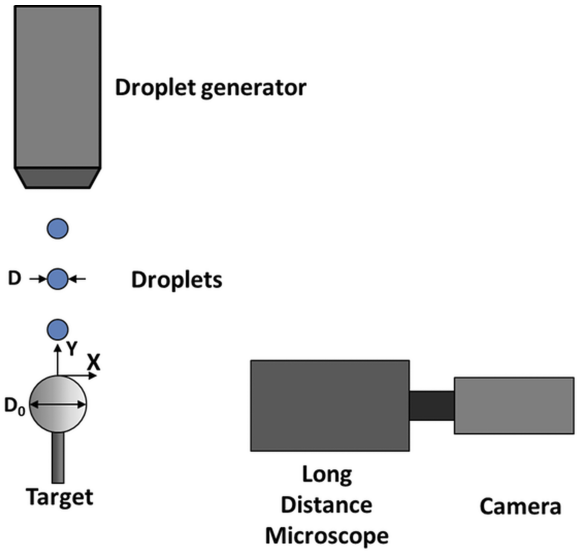


FIG. 3. Sketch of the experimental arrangement of the droplet-particle collision geometry and the imaging system.

of the impingement process. The magnification of the imaging system was about 2.5 μm/px, which provides sufficient resolution to record the outcomes of the collisions of the droplets on the particle (Fig. 3). The frame rate time required to temporally resolve the particle-droplet collisions, even at a modest resolution of 10 frames/collision at 10 kHz droplet generation, is 100 kHz. The required frame rate can be as high as 400 kHz for a temporal resolution of 20 frames/collision and a droplet generation frequency of 20 kHz. Such frame rates are beyond the capabilities of current high speed cameras at full resolution. For this reason, a phase shift was introduced between successive acquired images. This resulted in a considerable number of droplet-particle collisions taking place between successive frames. As it can be observed in the example of Fig. 4, the process was very repeatable and the full evolution of the droplet-particle collisions was captured.

Due to the fast evolution and the high magnification of the droplet-particle collision process, low shuttering time is critical to avoid motion blur. For this reason, back illumination was provided by an Nd-YAG laser exciting a Rhodamine WT dye solution in a cuvette (fluorescence lifetime of a few ns). In this way, exposure was effectively a few ns and the maximum displacement of all the liquid in the image was below a pixel. Therefore, no motion blur was observed in the tested flow conditions.

Two non-dimensional numbers are typically used to describe droplet impingement: the Weber number and the

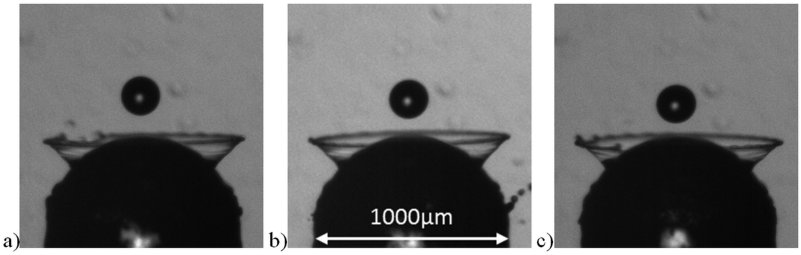


FIG. 4. Example of the repeatability of droplet-particle collisions. At least 1000 droplet impacts on the particle have taken place between successive images. The example shown is for $D_0 = 1000\,\mu$m, D ~ 196 μm, U = 12.1 m/s, Ω = 0.20, We = 391, and Oh = 0.0084.

Ohnesorge number. The Weber number is defined as

$$We = \frac{\rho U^2 D}{\sigma}, \tag{2}$$

where ρ is the liquid density, D is the droplet diameter, U is the droplet velocity before collision, and σ is the surface tension at the gas/liquid interface. The Weber number expresses the ratio of the inertial forces to the surface tension forces of the droplet. Here, the Weber number spanned between $92 < We < 1015$, making inertial effects more significant than surface tension effects.

The Ohnesorge number is defined as

$$Oh = \frac{\mu}{\sqrt{\rho \sigma D}}, \tag{3}$$

where μ is the droplet viscosity. The Ohnesorge number expresses the ratio of the viscous forces to the surface tension and inertial forces on the droplets and does not depend on the flow velocity. The Ohnesorge number was between $0.0070 < Oh < 0.089$, making surface tension effects greater than viscous effects.

The Reynolds number, which is the ratio of the inertial to viscous forces,

$$\mathrm{Re} = \frac{\sqrt{We}}{Oh} = \frac{\rho D U}{\mu}, \tag{4}$$

can also be used. The range of Re was between $1100 < \mathrm{Re} < 4550$. However, since the Reynolds number is a function of We and Oh, it does not provide any additional information on the description of the collision induced liquid flow.

An additional parameter is required to describe collisions of spherical surfaces. This is the droplet to particle diameter ratio

$$\Omega = \frac{D}{D_0}, \tag{5}$$

where D_0 is the target particle diameter. The droplet to particle diameter ratio was in the range of $0.09 < \Omega < 0.55$. For the smaller Ω, the particle approaches a flat surface in comparison to the droplet, while, for the larger Ω, the particle curvature is significant. Ω becomes 0 for the limiting case of droplet collision on a flat surface. The ranges of Ω for each of the three considered target particle sizes are not overlapping and are shown in Table II.

TABLE II. Range of droplet diameter ratio, Ω, for each particle diameter.

D_0 (μm)	Ω
500	0.36–0.55
1000	0.17–0.28
2000	0.09–0.14

TABLE III. Summary of the parameters of the current study.

U (m/s)	6–11
D (μm)	170–280
D_0 (μm)	500, 1000, and 2000
We	$92 < We < 1015$
Re	$1100 < Re < 4550$
Oh	$0.0070 < Oh < 0.0089$
Ω	$0.09 < \Omega < 0.55$

The full summary of the range of the study parameters is shown in Table III.

III. RESULTS AND DISCUSSION

A. Collision outcomes

The outcomes of the droplet-particle collisions are presented next. The observations of the flow development can be made free from any outside interference as long as the displaced liquid droplet remains mostly above the top half of the target particle. In locations below the target particle meridian, the particle support column or the liquid that is accumulating under the particle may start to interfere with the evolution of the collision.

The outcomes of the collisions can be classified into three categories, examples of which are shown in Figs. 5–7 for a particle of 500 μm diameter and droplets with diameter around 250 μm colliding with velocities from 6 m/s to 15 m/s. The location of the droplet is described by the polar angle ϕ, defined as the angle at the particle centre between the vertical and the base of the crown on the particle surface.

In the first type of collision [Fig. 5(a)], the droplet interacts with the spherical particle without any of its liquid detaching. There are three stages in the evolution of the collision. During the first stage, Fig. 5(a), contact between the droplet and the particle surface is established. Around the contact line, a disc from the droplet liquid is ejected. The disc expands radially outwards along the plane of impact. At the next stage, Fig. 5(b), the disc expands farther out covering the particle surface with a liquid film. The film front does not grow fast enough to attain any significant height above the surface of the particle. Due to the thickness of the film and the small height of the film front, the liquid film is stable and does not form a rim that can become unstable and break up. At the third stage, Fig. 5(c), the droplet has completely collapsed on the particle. All of the ejected liquid from the point of impact has also collapsed at this stage since it did not propagate fast enough to extend past the particle diameter. A liquid film is formed on the particle surface.

The second type of impact is shown in Fig. 6, which can be described as a crown type. In this case, a crown is formed which expands faster than it collapses on the particle surface. The process begins in the same way as the deposition of the droplet. During the initial contact between the droplet and the particle, a disc of liquid is ejected radially from the contact line [Fig. 6(a)]. Unlike the deposition case where the developing disc is thick and slow, in this case, the disc is thin and expands fast. As it expands outwards, it forms a crown. This can be observed by comparing Figs. 5(b) and 6(b). The shape of the droplet also changes and it can be seen that, by this stage, it has deformed considerably and has spread along the particle surface. The rate at which the crown grows is not fast enough to destabilise the rim. Therefore, no secondary droplets are produced from the droplet-particle collision due to splashing. However, as the spherical particle has a limited extent, the crown can grow to a diameter that is greater than the diameter of the particle. If this occurs before the crown rim reaches the particle equator,

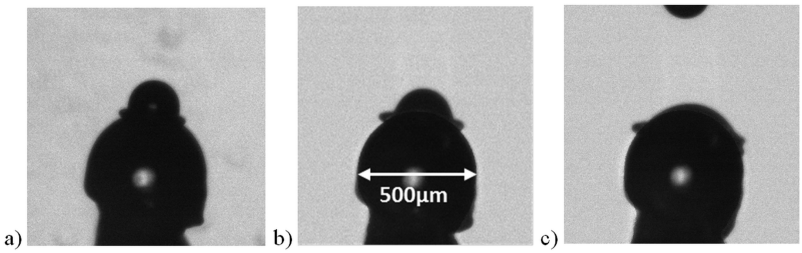


FIG. 5. Stages of impingement leading to deposition. (a) Initial contact at $\phi = 22°$. (b) Lamella growth at $\phi = 26°$. (c) Collapse at $\phi = 44°$. The example shown is for $D_0 = 500\ \mu$m, D ~ 210 μm, U = 6.1 m/s, $\Omega = 0.42$, We = 107, and Oh = 0.0081.

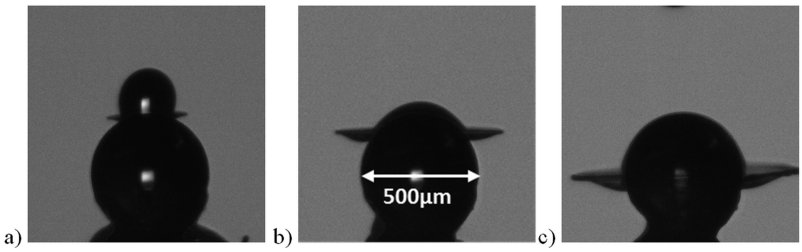


FIG. 6. Stages of impingement leading to overpass. (a) Initial contact at $\phi = 23°$. (b) The lamella growth at $\phi = 52°$. (c) Lamella projects beyond particle equatorial plane at $\phi = 102°$. The example shown is for $D_0 = 500\ \mu$m, D ~ 243 μm, U = 9.9 m/s, $\Omega = 0.49$, We = 328, and Oh = 0.0075.

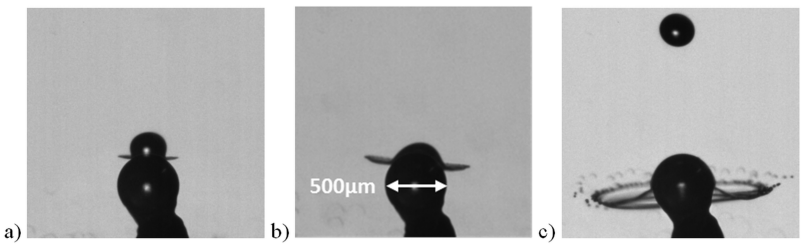


FIG. 7. Stages of impingement leading to splashing. (a) Initial contact at $\phi = 24°$. (b) The lamella growth at $\phi = 51°$. (c) Lamella breakup at $\phi = 94°$. The example shown is for $D_0 = 500\ \mu$m, D ~ 268 μm, U = 15 m/s, $\Omega = 0.54$, We = 830, and Oh = 0.0072.

the rim extends beyond the particle periphery and engulfs the particle rather than deposing on it. While the particle support post interferes with the evolution of the liquid flow at the base of the particle, it is reasonable to expect that, if the particle is dispersing freely in a flow, the liquid crown would form a jet downstream of the particle and droplets would pinch off. This type of small droplet formation cannot be expected from observations of collisions of droplets on flat surfaces.

The third type of droplet-particle collision is shown in Fig. 7. In this case, the initial impact is similar to the previous two. However, the ejected liquid expands radially much faster than the previous cases [Figs. 5(a) and 6(a)] and grows to a greater diameter, Fig. 7(a). This is attested by the expansion of the crown rim to almost the diameter of the solid particle in the case of the splashing collision, while, for the deposition and overpass, the expansion is less than about half a particle diameter, when the advancement of the crown base on the particle surface is the same at a polar angle of about $\phi = 22°$–$24°$ in all cases. A crown is formed as the disc expands, with the rim being higher than the expanding film front, Fig. 7(b). The rate at which the crown expands radially is sufficiently fast to initiate instabilities on the rim. As a result of the instabilities, cusps are formed from which droplets are ejected [Fig. 7(c)], as described for droplet collisions on flat surfaces (Yarin and Weiss, 1995). However, there are differences between the two cases. For a collision of a droplet on a flat surface, the liquid of the droplet is always ejected upwards, in the opposite direction of the droplet motion, as the flat surface prevents any other direction. The droplets that pinch off from the crown rim also fly out in the opposite direction of the original droplet motion. The situation changes in the case of the collision of the droplet with a spherical particle. In this case, the resistance of the particle surface to the droplet motion weakens as droplet to particle diameter ratio Ω increases since a greater proportion of the droplet is connected to the particle at an oblique angle. When the film front reaches the particle equator, the particle surface resistance to vertical motion due to impact diminishes. In that region, the direction of the front droplet liquid on the particle surface can have a component in the downward direction. This is demonstrated in Fig. 8, where the film ejection is seen to occur in a downward direction (the same as the droplet motion direction). This results in the development of a "U" shaped crown around the particle perimeter. This crown shape cannot be formed when droplets collide on flat surfaces. Despite its bent shape, the crown is stable at this stage and does not disintegrate soon after it is formed but continues to propagate along the particle surface even past the equator.

B. Mapping of the droplet-particle collision regimes

The droplet-particle collision regimes are summarized in Fig. 9 in terms of We and Oh. The splashing threshold is shown with a dashed line, and in general splashing occurs for We above 400. Deposition and droplet overpass occur at lower We. The influence of Oh is generally small. This is quite plausible since the magnitude of Oh is two orders of magnitude lower than unity and the viscous effects are outweighed by inertia and surface tension, which are captured well in We. Nevertheless, since the magnitude of Oh does not change by more than 30% in this investigation, its influence cannot be completely disregarded especially if more viscous droplets are considered and the value of Oh approaches unity.

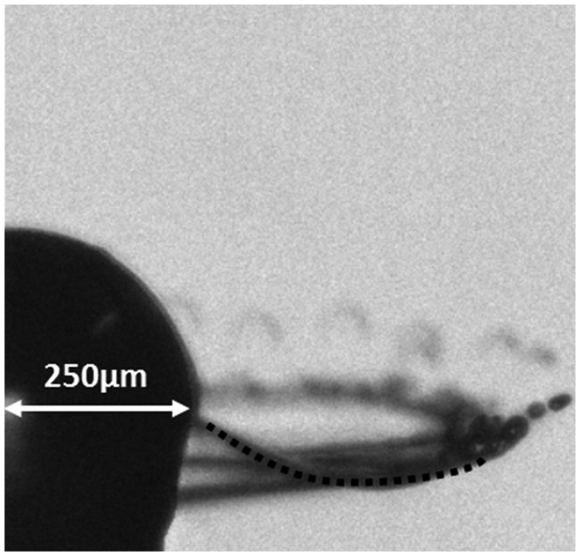


FIG. 8. Detail of the liquid film ejecting from the particle surface in Fig. 7(c). The satellite droplets formed can be observed. The dotted line highlights the curvature of the crown. The example shown is for $D_0 = 500\ \mu$m, D ~ 268 μm, U = 15 m/s, $\Omega = 0.54$, We = 830, and Oh = 0.0072.

The distinction between deposition (example of Fig. 5) and droplet overpass (example of Fig. 6) regimes is not immediately apparent in the Oh-We map because there is overlapping in the ranges of the two. The confusion can be alleviated by taking into account the particle diameter. Deposition always happens for the lowest values of We, but, as We increases above about 200, the collisions of the droplets with the 500 μm particle result in overpass. This is not the case for particles with diameters of 1000 μm and 2000 μm and the outcome of the collision remains in the deposition regime, until We becomes sufficiently large for splashing to occur. This can be understood by considering the droplet/particle ratio, Ω, which is too low for the larger particles, and the lateral expansion of the crown is not sufficient for the crown rim to clear the particle diameter before it collides on the particle surface.

The value of 400 for the Weber number found here for transition to splashing is in agreement with the findings of Wal *et al.* (2006), who reported a threshold of approximately $\sqrt{We > 20}$ for droplet impact on flat surfaces covered with a thin liquid film, and those of Cossali *et al.* (1997), who also reported a critical We of about 400 for Oh around 0.01. It is interesting to note that while the development of the droplet collision can be different depending on the diameter of the particle, it does not appear to influence the splashing threshold considerably. This is possibly because the splashing is dependent on the kinematic discontinuity of the expanding liquid film front on the particle surface. The size of the discontinuity is small compared to the diameter of the particle, and therefore in the locus of the discontinuity, the curvature of the particle does not change the process significantly.

The splashing threshold has been the focus of many investigations, and various splashing criteria have been suggested for droplet collisions on solid surfaces taking into account different descriptions of the flow. The most relevant ones of those to the current investigation are examined here.

For collisions of droplets on dry flat surfaces, Mundo *et al.* (1995) proposed a splashing threshold based on parameter K,

$$K = Oh\ \mathrm{Re}^{5/4}. \tag{6}$$

They proposed that splashing occurs for K greater than a critical value which depends on the surface characteristics. Hardalupas *et al.* (1999) extended this criterion to consider head-on collisions of droplets on dry spherical particles, and the definition of parameter K of Eq. (6) was modified to

$$K = g\,(\delta^*)\ Oh\ \mathrm{Re}^{5/4}, \tag{7}$$

with $g(\delta^*)$ being a parabolic function of the spherical particle curvature δ^*. The threshold value of K in the work of Hardalupas *et al.* (1999) was found in the region of $50 < K < 90$. The lower values were reported for increased particle curvature, meaning that decreasing particle diameter promotes splashing at a lower Re and Oh.

A comparison of threshold of the above criterion with the results of this investigation is shown in Fig. 10. The trend of the splashing threshold is qualitatively similar in both investigations. However, in all cases, splashing is predicted for droplet

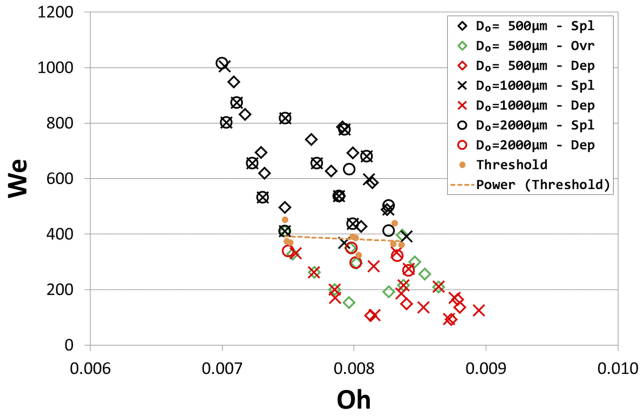


FIG. 9. Deposition (Dep), overpass (Ovr), and splash (Spl) regimes of droplet collision with spherical particles, examples shown in Figs. 5–7, respectively, in the domain of Oh-We. Splashing threshold, shown with a dashed line, appears at about We = 400.

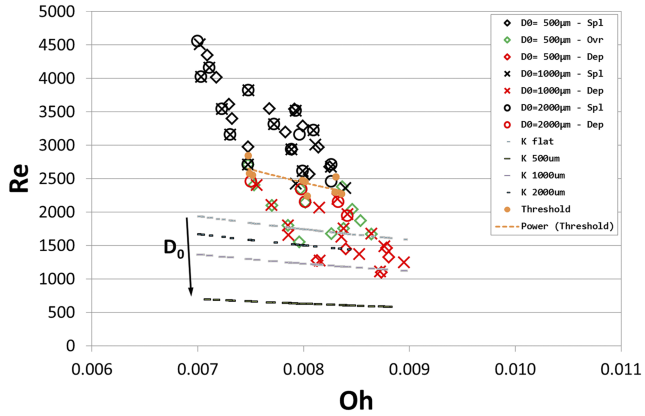


FIG. 10. Deposition (Dep), overpass (Ovr), and splash (Spl) regimes of droplet collision with spherical particles, examples shown in Figs. 5–7, respectively, in the domain of Re-Oh. The threshold estimated by Hardalupas *et al.* (1999) is shown for comparison.

collisions with dry particles at a lower Re than those found here. Even a collision of a drop with a flat dry surface is predicted to occur at a lower Re. In the case of droplet collision with a flat dry surface, it has been shown that increasing surface roughness reduces K considerably (Cossali *et al.*, 1997). The presence of the liquid film on the wall here appears to delay the shift of the splashing mechanism and the lessening of the interaction of the ejected film with the surface roughness.

In an experimental investigation by Yarin and Weiss (1995), the obtained splashing threshold for a series of droplets impacting at a frequency f on a wet, albeit flat surface, is given as a critical velocity U_{cr},

$$U_{cr} = 18\left(\frac{\mu\sigma^2 f^3}{\rho^3}\right)^{1/8}. \quad (8)$$

This threshold is independent of the droplet diameter and depends on the physical properties of the droplet and the collision frequency. It was suggested that the lack of influence of the droplet size is because the crown originates from the expanding liquid lamella on the flat surface after the droplet had fully collapsed, and therefore the original diameter of droplet is not relevant. According to the above criterion, the critical velocity of Eq. (8) is 9.6 m/s, 11.1 m/s, and 12.4 m/s, respectively, for the three droplet impact frequencies of 10 000 Hz, 15 000 Hz, and 20 000 Hz used here. A comparison of the two trends is presented in Fig. 11 in the domain of f and U. While, in the measurements presented here, the collision frequency does not appear to have a measurable effect on the splashing threshold, the criterion proposed by Yarin and Weiss (1995) appears to be relevant for spherical surfaces since the splashing threshold is found to be in the same region of U for both cases. The best agreement is observed for the droplet collision frequency of 15 000 Hz, where the threshold of Eq. (8) predicts exactly the observations, while for the other tested frequencies, there is a discrepancy of about 10%.

Finally, Liang *et al.* (2014) investigated the splashing threshold of single droplet collisions on wet spheres for Oh = 0.0026 and reported the splashing threshold as a critical Weber number. For Ω > 0.224, the threshold value of We was reported to be a linear function of Ω with a critical value of We increasing with Ω, meaning that smaller targets suppress splashing. For Ω < 0.224, the critical threshold was reported as a constant at about We = 124, meaning that, if the droplet diameter becomes smaller than about a quarter of the particle diameter, there is little difference in the collision between a droplet and a flat surface. The current results, along with the predictions of Liang *et al.* (2014), which were made for the same range of Ω as here, are shown in Fig. 12 in the domain of Ω and We. The predictions of Hardalupas *et al.* (1999) are also included for comparison. In this investigation, the splashing threshold was generally found to be around We = 400. When plotting the splashing threshold as a function of Ω, a small influence of Ω is indicated for Ω > 0.3 and a small increase of the critical value of We can be observed, which is not apparent in Fig. 9. Compared to the predictions made by Liang *et al.* (2014), the present splashing threshold of We is generally higher by at least a factor of two. However, there is good qualitative agreement and the trend of splashing threshold appears to be offset between the two investigations. Differences in the absolute scales might be attributed to the particulars of the experimental implementation, which may not be completely apparent. Also differences in the absolute scales between the two investigations may be a factor since the spatial scales were about 10 times greater in the work of Liang *et al.* (2014), while their collision velocities were about 3 times smaller. The predictions of Hardalupas *et al.* (1999) on the other hand are in disagreement with the findings of this investigation as far as the effect of Ω is concerned, with greater Ω resulting in a reduction of the splashing threshold. The difference in the trends is not immediately obvious since the surface curvature effect on the splashing threshold does not appear for the wetted surface until the surface curvature is substantial, while, in the case of the dry surface, the surface curvature has an immediate effect although this effect is more profound for greater surface curvatures (Ω > 0.2).

In the case of the droplet collision on the wet particle surface, the mechanism for splashing is the kinematic discontinuity. As long as the characteristics of the kinematic discontinuity are not altered by the particle curvature, the splashing of the

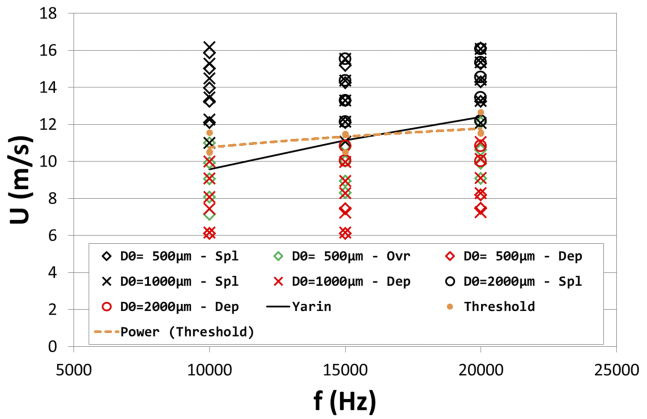


FIG. 11. Deposition (Dep), overpass (Ovr), and splash (Spl) regimes of droplet collision with spherical particles, examples shown in Figs. 5–7, respectively, in the domain of f-U. The splashing threshold estimated by Yarin and Weiss (1995) is shown for comparison.

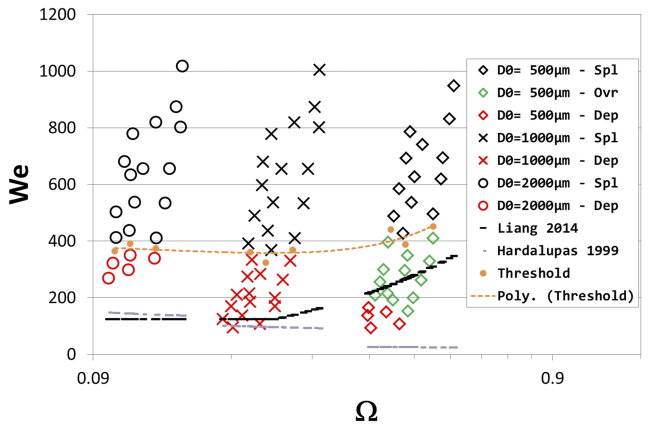


FIG. 12. Deposition (Dep), overpass (Ovr), and splash (Spl) regimes of droplet collision with spherical particles, examples shown in Figs. 5–7, respectively, in the domain of We-Ω. The threshold is described by a polynomial (Poly). The thresholds estimated by Liang *et al.* (2014) for wet impacts and by Hardalupas *et al.* (1999) for dry impacts are shown for comparison.

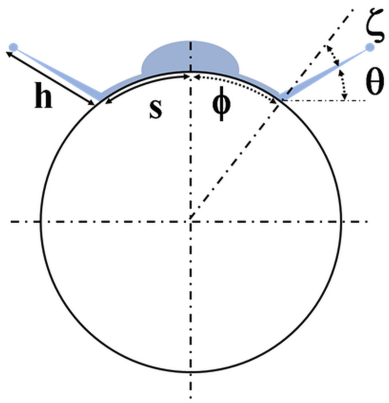


FIG. 13. Sketch defining the parameters used to characterise the crown. Lengths are shown with solid lines and angles are shown with dotted lines.

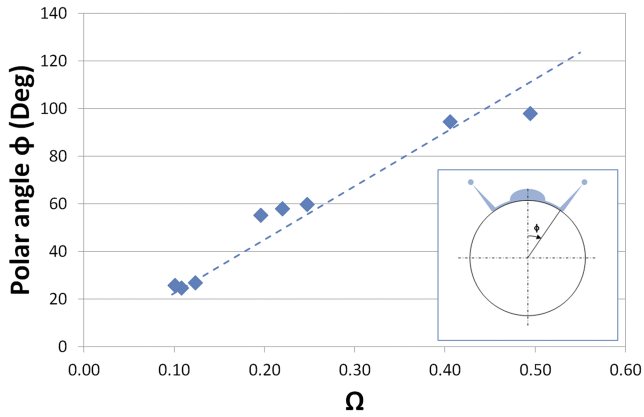


FIG. 15. Polar angle ϕ, defined in Fig. 10, at the onset of rim instability as a function of droplet to particle diameter ratio.

crown will not be severely affected. This does not appear to occur until Ω ~ 0.5, when the particle curvature is considerable and the deflection of the droplet liquid from the original direction is lower. Therefore, the acceleration of the film and hence the film velocity on the surface are lower, making the discontinuity less abrupt and splashing suppressed.

In the case of the dry particle, while the increasing curvature will have the same effect on the film acceleration, the effect of the perturbation due to surface roughness can be expected to be greater. As the liquid film propagates on the curved dry particle surface, it has momentum with a component that is normal to the surface and consequently a tendency to eject, which becomes greater as the surface curvature increases. Therefore, the surface roughness perturbations, which do not have a significant effect on the kinematic discontinuity, will promote the formation of a crown and splashing more so in the case of greater surface curvature.

C. Onset of instability on the crown rim

The outcomes of the droplet collision on the target particle have been described in Sec. III A and the splashing threshold has been determined in Sec. III B. In this section, the initiation of crown breakup is examined and the characteristics of the liquid film on the particle surface and the crown are described at the onset of the crown rim instability. Various parameters are utilised, which are shown schematically in Fig. 13. The polar angle ϕ is defined as the angle at the particle centre between the vertical and the base of the crown on the particle surface. A value of 0° denotes the north pole of the particle, while a value of 90° denotes the particle equator. The polar angle also describes the amount of coverage of the droplet by the film. The crown angle θ is the angle between the crown and the horizontal direction. A positive θ denotes ejection upwards and a negative θ denotes ejection downwards. The deflection angle ζ is defined between the crown and the normal to the particle surface at the base of the crown. A positive angle denotes that the crown is ejected in front of the surface normal and a negative angle denotes that the crown is ejected behind the surface normal. The arc of the liquid film from the north pole of the particle to the ejection front on the droplet surface is denoted as "s." The height of the crown is denoted as "h."

The focus is on the description of the crown at the splashing threshold, when the crown rim becomes unstable. This information is useful for the evaluation of numerical results and analytical approaches on the instability on the expanding crown. Also, these results can assist the optimisation of particle coating in different industrial processes.

Some examples of the crown at the instance of the rim destabilisation are shown in Fig. 14. In all cases (including those not shown) by the time the instability has appeared on the crown rim, the original droplet has collapsed on the particle. Therefore, no memory of the original droplet shape is retained when the instability forms and it can be argued that the splashing on the particle surface is due to the expansion of the liquid film as it has been proposed by Yarin and Weiss (1995) for splashing of droplets on flat surfaces.

The polar angle ϕ at the instance of the formation of the crown instability is presented in Fig. 15. For impacts between droplets and particles of comparative size (Ω ~ 0.5), the crown rim begins to destabilize after the liquid film front has been deflected considerably from its original direction and is in the vicinity of the particle equator. As Ω decreases, the rim begins to destabilize at progressively lower polar angles. For Ω around 0.2, the instability initiates at ϕ ~ 60°, while, for Ω around 0.1, which is the lowest considered here, the onset of rim instability occurs at ϕ ~ 20°. A linear fit results in a correlation coefficient of 0.93, which suggests a linear relationship between Ω and ϕ.

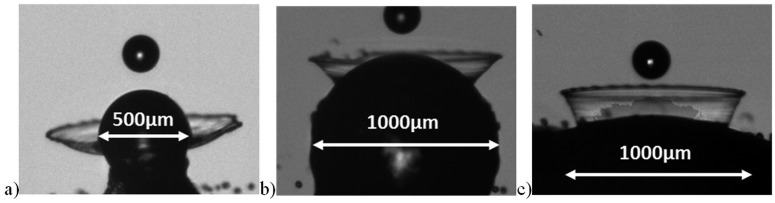


FIG. 14. Examples of initiation of crown rim instability for (a) D_0 = 500 μm, D ~ 203 μm, U = 13.2 m/s, Ω = 0.41, We = 488, and Oh = 0.0082, (b) D_0 = 1000 μm, D ~ 196 μm, U = 12.1 m/s, Ω = 0.20, We = 391, and Oh = 0.0084, (c) D_0 = 2000 μm, D ~ 202 μm, U = 12.2 m/s, Ω = 0.10, We = 412, and Oh = 0.0083.

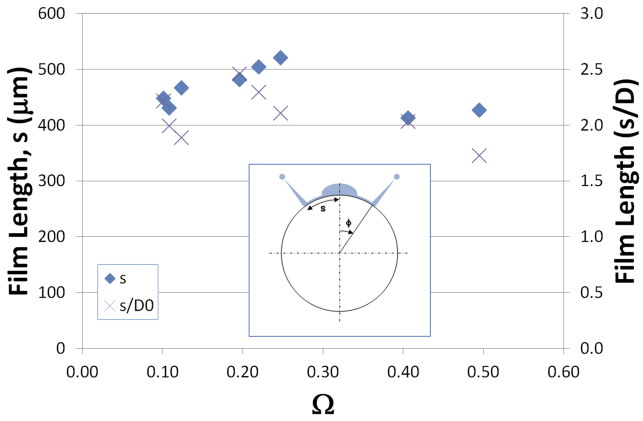


FIG. 16. Length of the liquid film on the particle surface at the moment of the onset of the rim instability as a function of droplet to particle diameter ratio. Rim instability sets when the film has propagated 400 μm–500 μm along the particle surface.

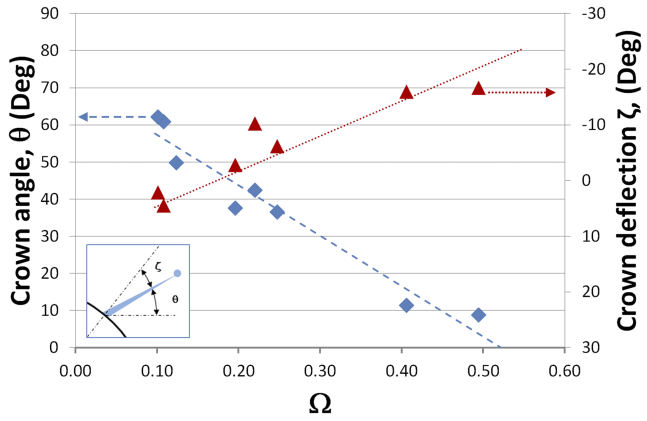


FIG. 17. Direction of the crown, defined by the angles θ and ζ of Fig. 13, at the onset of rim instability. For low particle-droplet ratio Ω, the crown is more vertical (diamonds on the left axis) and ejects in front of the surface normal (triangles on the right axis).

The distance s, which the liquid film front has traversed on the particle surface, is examined. In all cases, the rim instability onset occurs when the liquid film front traversed a distance of about 400 μm < s < 500 μm from the point of impact (Fig. 16). Consequently, the droplet-particle diameter ratio Ω does not appear to influence the length of the liquid film onset of instability. The length of the film, non-dimensionalised with the diameter of the droplet, is also considered to point out any trends that might depend on the droplet size. The normalised distance that is traversed until the onset of instability is about 2–2.5 times the diameter of the droplet and is also irrespective of Ω. It can, therefore, be claimed that the instability of the crown rim occurs when the film has traversed a distance of about 2 times the diameter of the droplet irrespectively of the diameter of the particle. The mainly constant length of the film may be explained by the largely constant velocity of the droplet impact shown in Fig. 11, which is close to the velocities suggested by Yarin and Weiss (1995) at the splashing threshold. As the droplets impinge with the same velocity, the expansion of the film on the surface of the particle develops similarly; therefore, the overall expansion of the film on the particle surface is more or less the same regardless of the particle size. Following this argument, the effect that the change of the particle diameter D_0 has on the polar angle ϕ becomes clear since ϕ is linearly proportional to D_0. Considering that, at the splashing threshold, the range of the droplet diameters is within 25% of their mean, the linear trend of the polar angle ϕ with the droplet-particle diameter ratio Ω can also be explained.

Following the description of the behaviour of the liquid film, the crown is examined next. The direction of the crown ejection θ is measured from the horizontal (Fig. 13). Therefore, a value of 0° represents ejection along the horizontal direction and a value of 90° represents ejection along the vertical direction. The ejection angle at the onset of instability is shown in Fig. 17 as a function of Ω. The droplet-particle diameter ratio has a definite effect on the crown ejection angle with the crown ejecting towards the horizontal direction for large Ω (small particles) and towards the vertical for small Ω (large particles). The trend can be approximated by a linear function.

While the ejection angle θ with respect to the horizontal shows the absolute direction of the ejection of the crown at the onset of rim instability, the deflection angle ζ, which is related to the polar and crown angles by the relationship $\zeta = \pi/2 - \phi - \theta$, between the crown and the normal to the particle surface demonstrates if the ejection is advanced or retarded to the kinematic discontinuity. On the secondary axis of Fig. 17, the deflection angle ζ is observed to occur after the kinematic discontinuity for large Ω (negative ζ) and progressively becomes slightly positive, as the particle surface becomes less curved at small Ω (positive ζ). To the best of the authors' knowledge, this effect has not been reported before. It shows that when the droplet diameter approaches the diameter of the particle, the propagation of the ejected crown is heavily affected by the change in the direction of the film front and, therefore, the history of ejection. At the point of impact, the ejection is along the horizontal as demonstrated in Figs. 5–8. Therefore, the deflection angle is 90° for all cases. However, as the liquid film front propagates on the particle surface, the crown becomes retarded with respect to the front, more so for greater values of Ω. As the instability sets at about the same distance s from the point of impact, the film front at the onset of instability has advanced by a greater amount for the larger Ω.

The analysis of the behaviour of the crown angle is complex even for droplet collisions with flat surfaces and there is no consensus on its modeling. The relationship proposed by Fedorchenko and Wang (2004) relating the crown angle to the non-dimensional film thickness was criticised by Yarin (2006). The relationship proposed by Roisman and Tropea (2002) is quite detailed but requires prior knowledge of the liquid film and crown velocities and thicknesses and is therefore difficult to confirm even for droplet impingement on flat surfaces. While the determination of the magnitude of the crown angle is difficult for droplet impingement on a flat surface, it is possible to argue how the crown angle will develop on a curved surface, as in the case of a particle, in relation to the crown angle of a droplet impact on a flat surface. Let us assume that, for a flat surface impact, the angle between the surface and the crown is θ_0. As the size and velocity of the droplets at the splashing threshold were found in Sec. III B to be fairly

constant, θ would not change significantly between cases. The corresponding deflection angle for the flat surface would be $\zeta_0 = \pi/2 - \theta_0$. As the spreading droplet film expands on the particle surface, the direction of the surface normal changes with ϕ. If the crown was free to eject at the same direction ζ_0 in relation to the surface normal as before, the direction of ejection would be $\theta = \pi/2 - \phi - \zeta_0$. This would make the crown angle a linear function of the polar angle ϕ, as is shown in Fig. 17. However, ζ also changes with ϕ. Because of the change of the polar angle ϕ as the crown propagates, the ejected liquid at the base of the crown will be ejected in a more forward direction in relation to the downstream liquid. Consequently, it will be pulled back with respect to the surface normal, resulting in a decrease of the deflection angle. This effect can be expected to be proportional to the curvature of the particle and, therefore, the crown deflection angle ζ will decrease proportionally to Ω.

Finally, the crown height, at which the crown instability initiates, is presented in Fig. 18. The range of values of h is between 150 μm and 350 μm and its magnitude appears to have a linear dependence on Ω with higher values of h obtained for larger Ω. The dependence on Ω can be explained by considering the crown ejection, which occurs at increased ejection angles θ. The original droplet velocity is downwards. A higher ejection angle θ means that the change in the momentum of the droplet liquid and, therefore, the force acting upon it is greater than the force acting on a laterally ejected jet. Consequently, the resistance to the ejection of the crown is greater and the outwards expansion of the crown is suppressed. Conversely, for an increased value of Ω, as the droplet size approaches the particle size, ejection takes place at low θ and the resistance of the particle surface to the expansion of the crown is reduced. Therefore in the latter case, the crown expands with less resistance and obtains a greater height. The above is supported by the fairly good correlation (correlation coefficient of 0.87) between the lengths of the arc from the base of the crown to the horizontal from the north pole of the particle. This shows that the length of the arc is proportional to the height that is added to the crown due to the curvature of the particle surface, which is constantly recessing. Therefore, the surface curvature of the particle acts to stretch the crown, adding to its total height.

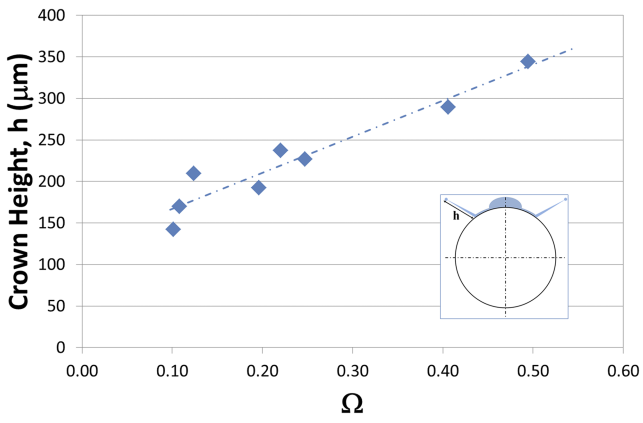


FIG. 18. Crown height measured from the sphere surface to the rim.

The characteristics of the crown that were presented in the preceding paragraphs are important for the accurate modeling of the splashing process as it marks the formation of the jets from which the fine droplets will be produced. It is also important for the evaluation of numerical models, which simulate the collision of droplets on particles, as it has been stressed by Zhang *et al.*, 2010 who demonstrated that simulations must be coupled with experimental work to fine tune the parameters of the simulation to obtain the correct prediction of the wavelength on the crown rim.

In practical terms, the height of the crown at the onset of instability demonstrates the distance from the droplet surface from which the droplets will begin to form. Consequently, if the crown height is higher, which occurs for higher Ω, the generated droplets will escape more easily from the vicinity of the particle to form fine particles in a spray dryer installation. When considering that, for higher Ω, the droplets are released close to the equator of the solid particle, the chance to escape collision with the target particle increases further. It can then be claimed that, in spray dryers, the generation of fine particles from droplet-particle collisions occurs mainly close to the top of the dryer, where the particles have not had a change to aggregate and grow in size and the droplet-particle diameter ratio remains high.

The direction of the crown in relation to the target surface is also important, as it is the direction at which the jets will begin to emerge from the crown rim. This direction becomes progressively tangential to the horizontal as the droplet-particle diameter ratio increases. This shows that the interaction of the liquid droplet and the film on the particle surface changes with Ω, and Ω needs to be taken into account in the analytical examination of the kinematic discontinuity. While it can be suggested that the change of the angle is only due to the curvature of the particle and the crown is still ejected normal to the curved surface, the deflection from the particle surface normal is more retarded as Ω increases, and therefore the effect of the surface curvature should not be ignored. In practical terms, the ejection angle will determine the trajectory of the fine droplets. In the practical application, a crown ejection angle sideways to the particle, as it occurs for higher droplet-particle diameter ratios, increases the probability that the generated droplets after the droplet impact will clear the target particle. This is the case for head-on collisions, which are examined here. For oblique droplet-particle collisions, which can also occur in a practical application, the crown development will be affected and the probability of the generated fine droplets clearing the particle will change. On the side of the crown ejecting towards the particle, the probability of the fine droplets clearing the particle will decrease, while on the side of the crown ejecting away from the particle, the probability will increase. The net effect will depend on the collision angle and it is possible that more or less material will be deposited on the particle surface. The exact details of this process, however, cannot be determined by the current investigation.

Finally, the length of the film on the particle surface can be considered equivalent to the base diameter of the crown during impact on flat surfaces. As it is described by the review of Liang and Mudawar (2016), there is no complete consensus

on the evolution of the crown base for collisions of droplets on flat surfaces, but generally it grows as a function of time with an exponent around 0.5 or less. In the present investigation, while the measurements were not time resolved due to the small scales involved, it was found that the film length was more or less invariant at the commencement of instability. As such, it can be inferred that there may be a correlation between the perturbation of the crown at its base due to the length of the travelled distance and the commencement of instability which may be taken into account when considering the development of the Rayleigh Plateau instability, which is considered the dominant instability mechanism (Liang and Mudawar, 2016).

D. Proper orthogonal decomposition of droplet-particle collisions

Further to the examination of particular characteristics of the crown by a direct measurement on the images, the sequences of the acquired images of each measurement at the splashing threshold were analysed by means of Proper Orthogonal Decomposition (POD). The POD method is a statistical procedure that decomposes a set of multidimensional datasets, in our case sets of images, and produces a new basis for the description of the data. The POD method when applied to multiphase flow images has been shown to accurately identify flow structures better than the direct observation of individual images (Arienti and Soteriou, 2009; Charalampous and Hardalupas, 2014). The procedure of analysing an image dataset with the POD method can be summarised as follows:

1. Calculation of the mean image of the dataset.
2. Subtraction of the mean image from each individual image to obtain the set of deviations from the mean.
3. Calculation of the covariance matrix of the deviation dataset.
4. Calculation of the eigenvectors and eigenvalues of the covariance matrix.
5. The eigenmodes of the covariance matrix are the POD modes.
6. The eigenvalue that corresponds to each of the POD modes is commonly referred to as the energy of that mode.
7. The POD modes are ranked in the order of descending eigenvalues.

From the description of the procedure, it can be understood that the POD modes are linearly uncorrelated and that the first POD mode captures the largest amount of image intensity variability, while each successive POD mode captures progressively lower image intensity variability. These two properties make the use of the POD method attractive as the information in each POD mode is unique and the POD modes are ranked based on the amount of information they capture. An example of POD analysis of an image dataset is shown in Fig. 19. The first two rows show an example of images from all the stages of droplet-particle collision in the dataset. The bottom row shows the first POD modes.

The POD modes are composed of patterns of alternating red and green nodes in the image regions along the droplet trajectory and in the image regions where the crown develops. Each node identifies a region where there is coherent spatial distribution of liquid. For example, the red nodes of the first POD mode show the location of the droplet and the crown when the droplet just impinges on the particle surface. This is very similar to the first image sample in Fig. 19. The green nodes in the same image identify the locations in the image where the droplet and the crown appear when the progress of impingement is similar to the fourth image in Fig. 19. The green nodes of the second POD mode show the location of the droplet and the crown when the droplet is partially collapsed, which is similar to the second image sample in Fig. 19. Higher-order POD modes capture progressively fine details of the droplet-particle impact. For example, the POD mode 3 in Fig. 19 shows a refinement of the scales of the POD nodes to about half the scales of modes 1 and 2, while mode 6 (fourth image in the bottom row of Fig. 19) shows a finer refinement. The individually emerging droplets from the crown rim, as seen in the fourth image of Fig. 19, are not captured by any of the first POD modes, as they are minute compared to the scales that these POD modes resolve. The particle itself does not appear directly but can be clearly identified as the spherical black void within the nodes of the POD modes. Therefore, for each measured image, the first POD modes identify the structures in the images, which are more prominent. While arguably some of the information that can be obtained from the first POD modes may also be obtained by the observation of individual images across the dataset, the POD mode has the advantage that measurements, such as the height of the crown, can be obtained directly from a single POD mode.

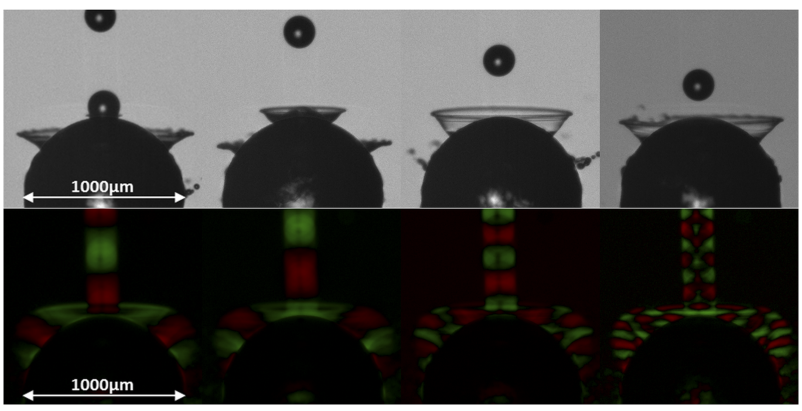


FIG. 19. Example of the droplet impingement sequence and the POD analysis for D_0 = 1000 μm, D ~ 196 μm, U = 12.1 m/s, Ω = 0.20, We = 391, and Oh = 0.0084. Top row: the example of images from the dataset. Bottom row: POD modes 1, 2, 3, and 6 showing progressively finer details of the droplet-particle impingement process.

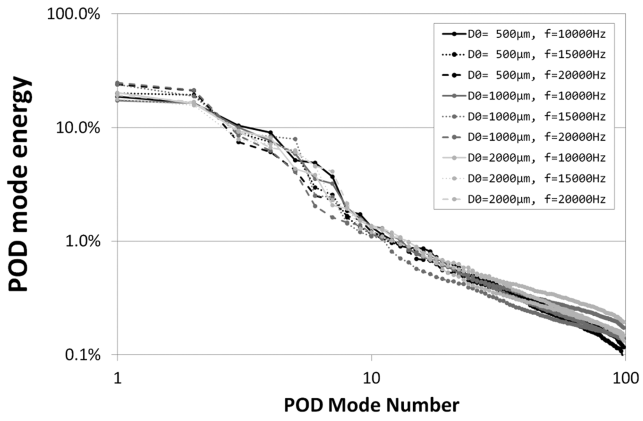


FIG. 20. Distribution of the energy of the POD modes at the splashing threshold. The first two modes contain most of the energy. The energy of subsequent modes decreases quickly. The labels indicate the diameter of the target particle and the frequency of the droplet impacts.

The importance of the first POD modes is also highlighted by the fraction of the total POD mode energy captured by them as can be seen in Fig. 20 by the distribution of the POD mode energy of the flow conditions at the splashing threshold. The first two modes, each contains between 15% and 24% (35%–45% between them) of the total energy, while the energy contained in subsequent modes decreases rapidly. For example, mode 3 captures less than 10% of the total energy. As the first modes also capture the largest scale phenomena, which can be related to the development of the crown, the present POD examination will focus on these two modes.

Examples of the first two POD modes for each particle size class are presented in Fig. 21 for the corresponding flow conditions of the examples shown in Fig. 14.

For droplet collision on small particles [example shown for $\Omega \sim 0.4$, Fig. 21(a)], the distribution of the POD nodes shows that the particle becomes completely engulfed by the crown, which expands to a maximum at around the equator of the particle and, from that point, it continues to flow downstream. For intermediate sized particles [example shown for $\Omega \sim 0.2$, Fig. 21(b)], the POD modes show that the crown initially expands laterally but then moves downwards until the crown recedes and collapses at around the equator of the particle. Finally, for droplet collision on large particles, the example shown for $\Omega \sim 0.1$ [Fig. 21(c)], the crown collapses at the particle surface.

The droplet-particle collision process is captured by the first two POD nodes on the large scale in discrete stages, as can be observed by the succession of the red and green nodes. The POD node at the north pole of the particle captures the locus of the droplet impact on the particle surface and defines the region of crown development. The subsequent mode in all cases shows the locus of the crown after the impact phase was completed. Every successive mode shows the locus of subsequent non-overlapping regions of the crown. This description of the splashing process by the POD modes can be advantageous when modeling the splashing of a droplet, as it offers an *a priori* template of the location of the liquid and the coarse features of the splash over which a computational mesh can be refined, while in the regions, where there is absence of droplet or crown development, can be coarsely meshed. Considering that the positively correlated regions account for only half of the imaged domain, the calculation time could be reduced significantly.

Some of the overall characteristics of the ejected liquid from the droplet-particle collision can be determined by analysing the single POD modes, instead of processing individual images. The maximum height of the ejected liquid from the particle top surface is examined here, as this property has also been studied for collisions of droplets on flat surfaces and comparison can be made. In the case of droplet collision on small particles [example shown for $\Omega \sim 0.4$, Fig. 21(a)], the crown rim rises minimally above the north pole of the particle. For progressively increasing particle diameters, the POD mode begins to expand in the vertical direction [example shown for $\Omega \sim 0.2$, Fig. 21(b)], while for droplet impingement on large particles [example shown for $\Omega \sim 0.1$, Fig. 21(c)], the POD mode indicates significant height reflecting the crown behaviour. Quantitatively, the crown height is presented in Fig. 22. The relationship can be described by an exponential trend. The trend predicts that the maximum height of the

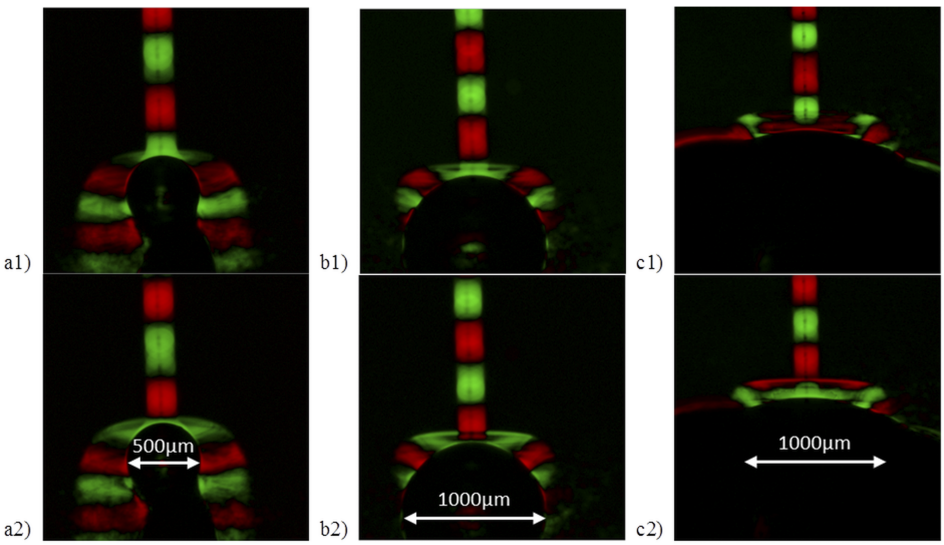


FIG. 21. POD modes 1 and 2 showing the formation and the crown for (a) $D_0 = 500\,\mu$m, $D \sim 203\,\mu$m, $U = 13.2$ m/s, $\Omega = 0.41$, We = 488, and Oh = 0.0082, (b) $D_0 = 1000\,\mu$m, $D \sim 196\,\mu$m, $U = 12.1$ m/s, $\Omega = 0.20$, We = 391, and Oh = 0.0084, (c) $D_0 = 2000\,\mu$m, $D \sim 202\,\mu$m, $U = 12.2$ m/s, $\Omega = 0.10$, We = 412, and Oh = 0.0083. The green and red regions denote areas of alternating presence of liquid.

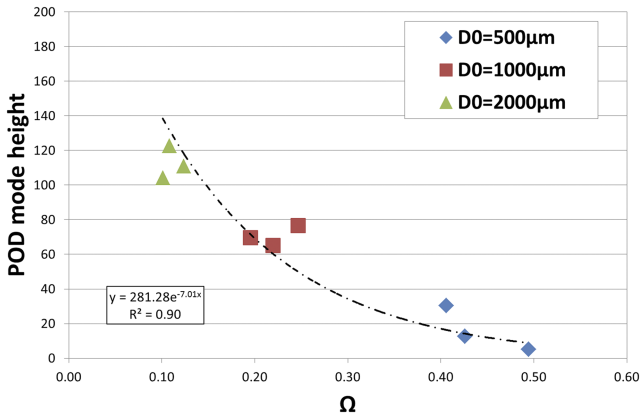


FIG. 22. Height of the POD modes at the splashing threshold.

ejected liquid will be about 280 μm when $\Omega = 0$ (flat surface). The measurements of Cossali *et al.* (2004) determined that the maximum height of the crown for collisions of droplets on wet flat surfaces covered by a thin film and under the same Weber number as here (We ~ 400) is about 35% greater than the droplet diameter. Considering the size of the examined droplets here, the prediction of Cossali *et al.* (2004) gives a maximum height of about 300 μm, which is within 10% to the prediction of the POD analysis.

IV. CONCLUSIONS

An investigation was undertaken to examine the physics of the droplet-particle collisions. The Weber, Ohnesorge, and droplet-particle diameter ratio numbers of the flow were varied within the ranges of $92 < We < 1015$, $0.0070 < Oh < 0.0089$, and $0.09 < \Omega < 0.55$. The investigation focused on the outcomes of the collisions between liquid droplets and spherical particles and on the description of the crown development at the threshold of splashing. The findings are as follows:

1. Three outcomes of droplet-particle collisions are possible. Two of them are deposition and splashing, which can also be observed when droplets collide with flat surfaces. A third outcome, unique to droplet-particle collisions, is the overpass type, where a stable crown is formed that propagates around the particle and clears the equatorial plane without breaking up. This type of outcome was only observed when the droplet diameter became comparable to the particle diameter, $\Omega > 0.3$.
2. Splashing of the droplet on the particle occurs for Weber numbers in the region of We = 400. The Weber number is defined as $We = \frac{\rho U^2 D}{\sigma}$, where ρ is the liquid density, D is the droplet diameter, U is the droplet velocity before collision, and σ is the surface tension at the gas/liquid interface without much influence of the particle size. This splashing threshold is in agreement with previous investigations of droplet collisions on flat surfaces (Cossali *et al.*, 1997; Wal *et al.*, 2006). The agreement suggests that when the crown develops on a particle surface, the mechanism of breakup remains unchanged.
3. High droplet-particle diameter ratios ($\Omega > 0.3$) were found to only slightly suppress splashing by increasing the critical value of We to about 450.
4. The splashing threshold proposed by Liang *et al.* (2014) for collisions of droplets on wet particles was in qualitative agreement with the current findings. However, the critical values of We found here are over two times greater than those reported by Liang *et al.* (2014).
5. The splashing threshold proposed by Hardalupas *et al.* (1999) for collisions of droplets on dry particles was in disagreement with the findings of this investigation since it suggests that increasing Ω promotes splashing.
6. At the splashing threshold, the instability at the crown rim was found to initiate when the film front travelled a distance of about 400 μm–500 μm independently of particle size. This is equivalent to about 2 droplet diameters.
7. At the splashing threshold, the direction of the crown ejection angle is significantly affected by the droplet-particle diameter ratio Ω and it can be described by a linear function of Ω. For low Ω, ejection is towards the vertical and, as Ω increases, the ejection direction changes towards the horizontal.
8. At the splashing threshold, the height of the crown at the onset of instability was found to be in the range of 150 μm–350 μm. It depends on Ω with greater crown heights obtained for larger Ω as the greater extent of the droplet crown is free to expand in the lateral direction.
9. Proper orthogonal decomposition analysis of the datasets at the threshold of splashing showed that the large scale characteristics of the development of the droplet-particle collision and the ejected liquid can be captured by the first two POD modes. This may assist the development of simplified computational models for droplet-particle collisions.
10. The maximum height of the ejected liquid above the particle is found from the POD modes to be in the range of 0 μm to 120 μm and an exponential function of Ω. The proposed function agrees within 10% with the maximum reported height for droplet collisions on flat surfaces by Cossali *et al.* (2004).

ACKNOWLEDGMENTS

Support from the Engineering and Physical Sciences Research Council (EPSRC), Grant No. EP/K019732/1, and P&G is acknowledged.

Arienti, M. and Soteriou, M. C., "Time-resolved proper orthogonal decomposition of liquid jet dynamics," Phys. Fluids **21**(11), 112104 (2009).

Baker, C. G. J. and McKenzie, K. A., "Energy consumption of industrial spray dryers," Drying Technol. **23**(1-2), 365–386 (2005).

Bakshi, S., Roisman, I. V., and Tropea, C., "Investigations on the impact of a drop onto a small spherical target," Phys. Fluids **19**(3), 032102 (2007).

Barnes, H. A., Hardalupas, Y., Taylor, A. M. K. P., and Wilkins, J. H., *An Investigation of the Interaction Between Two Adjacent Impinging Droplets* (ILASS-Europe'99, Toulouse, 1999), pp. 1–7.

Brenn, G., Durst, F., and C. Tropea, "Monodisperse sprays for various purposes–their production and characteristics," Part. Part. Syst. Charact. **13**(3), 179–185 (1996).

Brenn, G. and Frohn, A., "Collision and coalescence of droplets of various liquids," J. Aerosol Sci. **20**(8), 1027–1030 (1989).
Chandra, S. and Avedisian, C. T., "On the collision of a droplet with a solid surface," Proc. R. Soc. A **432**(1884), 13 (1991).
Charalampous, G. and Hardalupas, Y., "Application of proper orthogonal decomposition to the morphological analysis of confined co-axial jets of immiscible liquids with comparable densities," Phys. Fluids **26**(11), 113301 (2014).
Cossali, G. E., Coghe, A., and Marengo, M., "The impact of a single drop on a wetted solid surface," Exp. Fluids **22**(6), 463–472 (1997).
Cossali, G. E., Marengo, M., Coghe, A., and Zhdanov, S., "The role of time in single drop splash on thin film," Exp. Fluids **36**(6), 888–900 (2004).
Fedorchenko, A. I. and Wang, A.-B., "On some common features of drop impact on liquid surfaces," Phys. Fluids **16**(5), 1349–1365 (2004).
Hardalupas, Y., Taylor, A. M. K. P., and Wilkins, J. H., "Experimental investigation of sub-millimetre droplet impingement on to spherical surfaces," Int. J. Heat Fluid Flow **20**(5), 477–485 (1999).
Huntington, D. H., "The influence of the spray drying process on product properties," Drying Technol. **22**(6), 1261–1287 (2004).
Liang, G., Guo, Y., Mu, X., and Shen, S., "Experimental investigation of a drop impacting on wetted spheres," Exp. Therm. Fluid Sci. **55**, 150–157 (2014).
Liang, G. and Mudawar, I., "Review of mass and momentum interactions during drop impact on a liquid film," Int. J. Heat Mass Transfer **101**, 577–599 (2016).
Masters, K., *Spray Drying Handbook* (Longman Scientific & Technical, 1991).
Mercer, A. C., "Improving the energy efficiency of industrial spray dryers," J. Heat Recovery Syst. **6**(1), 3–10 (1986).
Mundo, C., Sommerfeld, M., and Tropea, C., "Droplet-wall collisions, experimental studies of the deformation and breakup process," Int. J. Multiphase Flow **21**(2), 151–173 (1995).
Orme, M., "Experiments on droplet collisions, bounce, coalescence and disruption," Prog. Energy Combust. Sci. **23**(1), 65–79 (1997).
Pawar, S. K., Henrikson, F., Finotello, G., Padding, J. T., Deen, N. G., Jongsma, A., Innings, F., and Kuipers, J. A. M. H., "An experimental study of droplet-particle collisions," Powder Technol. **300**, 157–163 (2016).
Pergamalis, H., *Droplet Impingement onto Quiescent and Moving Liquid Surfaces* (Imperial College, 2002).
Podvysotsky, A. M. and Shraiber, A. A., "Coalescence and break-up of drops in two-phase flows," Int. J. Multiphase Flow **10**(2), 195–209 (1984).
Qian, J. and Law, C. K., "Regimes of coalescence and separation in droplet collision," J. Fluid Mech. **331**, 59–80 (1997).
Rioboo, R., Bauthier, C., Conti, J., Voué, M., and De Coninck, J., "Experimental investigation of splash and crown formation during single drop impact on wetted surfaces," Exp. Fluids **35**(6), 648–652 (2003).
Rioboo, R., Marengo, M., and Tropea, C., "Time evolution of liquid drop impact onto solid, dry surfaces," Exp. Fluids **33**(1), 112–124 (2002).
Rioboo, R., Tropea, C., and Marengo, M., "Outcomes from a drop impact on solid surfaces," Atomization Sprays **11**(2), 155–165 (2001).
Roisman, I. and Tropea, C., "Impact of a drop onto a wetted wall, description of crown formation and propagation," J. Fluid Mech. **472**, 373–397 (2002).
Roisman, I. V., Horvat, K., and Tropea, C., "Spray impact, rim transverse instability initiating fingering and splash, and description of a secondary spray," Phys. Fluids **18**(10), 102104 (2006).
Schneider, J. M. and Hendricks, C. D., "Source of uniform-sized liquid droplets," Rev. Sci. Instrum. **35**(10), 1349–1350 (1964).
Schneider, J. M., Lindblad, N. R., and Hendricks, C. D., "An apparatus to study the collision and coalescence of liquid aerosols," J. Colloid Sci. **20**(6), 610–616 (1965).
Wal, R. L. V., Berger, G. M., and Mozes, S. D., "The splash/non-splash boundary upon a dry surface and thin fluid film," Exp. Fluids **40**(1), 53–59 (2006).
Wang, A.-B. and Chen, C.-C., "Splashing impact of a single drop onto very thin liquid films," Phys. Fluids **12**(9), 2155–2158 (2000).
Yarin, A. L., "Drop impact dynamics, splashing, spreading, receding, bouncing. . . ," Annu. Rev. Fluid Mech. **38**(1), 159–192 (2006).
Yarin, A. L. and Weiss, D. A., "Impact of drops on solid surfaces, self-similar capillary waves, and splashing as a new type of kinematic discontinuity," J. Fluid Mech. **283**, 141–173 (1995).
Zhang, L. V., Brunet, P., Eggers, J., and Deegan, R. D., "Wavelength selection in the crown splash," Phys. Fluids **22**(12), 122105 (2010).